Optimisation-Deposition and Conversion of Lead Halide Thin Films to 2D Metal Halide Perovskite Thin Films via Low-Pressure CVD

M.S.L. Mthimkulu[1,2], S. Ngqoloda[2,3], C.J. Arendse[2], M.L.A. Letswalo[1], B.M. Sondezi[1]

[1]Department of Physics, University of Johannesburg, Johannesburg 2006, South Africa
[2]Department of Physics and Astronomy, University of the Western Cape, Bellville 7535, South Africa.
[3]Advanced Materials Division, Mintek, Randburg 2169, South Africa.

E-mail: bmsondezi@uj.ac.za and letswalom@uj.ac.za

Abstract. Three-dimensional (3D) metal halide perovskites (MHPs) are recognised as a prime candidate for optoelectronic devices, thanks to its excellent optical and electrical properties, as well as the ease of synthesis techniques. However, the 3D MHPs are prone to degradation, two-dimensional (2D) MHP have proven to be more stable. Herein, 2D MHP thin films were synthesised by converting lead bromide ($PbBr_2$) thin films into 2D MHP thin films using a sequential two-step low-pressure chemical vapour deposition (LPCVD) method. The first step involved depositing $PbBr_2$ thin films on glass/FTO/TiO_2 substrates. The second step exposed the as-prepared $PbBr_2$ thin films to phenyl-ammonium iodide (PEAI) vapour at two different temperatures of 170 °C and 190 °C during the conversion process. The structural and optical properties of the converted thin films were characterised using X-ray diffraction (XRD), ultraviolet-visible (UV-Vis), and photoluminescence (PL) spectroscopy. The results showed that the converted thin films did not fully convert to 2D MHPs, as evidenced by the presence of lead iodide (PbI_2) diffraction peaks in the XRD patterns. The optical properties indicate the partial formation of 2D MHPs with a stoichiometry of $(PEA)_2PbBr_xI_{4-x}$ ($0 \leq x < 1$). The results suggest that the conversion temperature of 170 °C is more suitable for obtaining high-quality 2D MHP thin films due to the lower defect density.

1. Introduction

Three-dimensional (3D) metal halide perovskite (MHP) has been known as an emerging semiconductor since Kojima and colleagues used it as a photosensitiser in dye-sensitised solar cells in 2009, reporting a power conversion efficiency (PCE) of 3.1% [1]. The exceptional optical and electrical properties of the 3D MHP, including tunable direct band gap, ambipolar charge transport, low nonradiative recombination rates, and high absorption coefficient, have led to a significant increase in PCE over the past two decades, reaching over 25.5% [2, 3].

Silicon (Si) remains the predominant choice in optoelectronic devices due to its abundance and well-known semiconductor properties. 3D MHP thin films have proven to be simpler to synthesise compared to Si, lowering

production costs. Together with the flexibility of the 3D MHP, intense research has been conducted into the perovskite material [4, 5].

The general stoichiometry of 3D MHPs is ABX_3, where A is an organic monovalent cation like methylammonium (MA^+, $CH_3NH_3^+$), B is a divalent metal cation, like lead (Pb^{2+}), and X is a monovalent halogen anion, like bromine (Br^-) [7, 8]. The B cation is coordinated with six X anions to form a $[BX_6]^{-4}$ octahedron. Each octahedron at the unit cell's corners shares an X anion to form a continuous 3D lattice. The A cation is enclosed between four octahedra and has 12 X anions forming a cuboctahedron [6].

Despite perovskite-based solar cells reaching a validated PCE of over 25% [9], 3D MHPs degrade in the presence of heat, light, and moisture due to their inherent chemical and structural instabilities, making it challenging to incorporate them into commercial devices. These difficulties highlight the pressing need for more reliable and affordable substitutes, which is fueling the intense study of 2D MHP [9, 13].

2D MHP has a general stoichiometry of $(A')_2A_{n-1}B_nX_{3n+1}$ ($n \in \mathbb{Z}^+$) where A' represents a large organic cation such as phenethyl-ammonium (PEA^+, $C_8H_9NH_2^+$), A, B and X represent the same ions as in the 3D MHP and n refers to the number of the metal halide octahedral units, where the limit $n = \infty$ relates to 3D MHP. The A' cation is large and cannot fit in the gap between the metal halide octahedra, unlike the smaller A cation, which occupies these gaps. The A' cation behaves as an insulating layer separating the octahedral units, which are connected by halide anions that share corners. One way to conceptualise the geometry of the 2D MHP is as a slice of the 3D MHP structure across the <100> crystallographic directions [13, 15].

The nearly constant conductivity of the $[BX_6]^{-4}$ octahedra layer and the insulation of the organic spacer layer give rise to the natural multiple quantum well (MQW) structure of 2D MHPs, where the perovskite inorganic layer functions as a "well" and the organic spacer layer as a "wall" [16]. Excitons, rather than electrons and holes, are formed when a 2D MHP is excited because of the quantum confinement effect, which raises the binding energy [16, 17]. The performance of optoelectronic devices can be enhanced by utilising these 2D MHP properties.

This study uses a sequential two-step low-pressure chemical vapour deposition (LPCVD) method to synthesise $(PEA)_2PbBr_yI_{4-y}$ ($0 \leq y \leq 4$) 2D MHP thin films. The first step is the deposition of lead bromide ($PbBr_2$) thin film on glass/FTO/TiO_2 substrates, followed by the second step, which is to expose the as-deposited $PbBr_2$ thin film to phenethyl-ammonium iodide (PEAI) vapour for conversion of the $PbBr_2$ thin film into a 2D MHP thin film. The furnace was set to two distinct temperatures, 170 °C and 190 °C, to investigate the conversion temperature.

2. Experimental

2.1. Substrate preparation

Glass substrates coated with fluorine-doped tin oxide (FTO) (purchased from Techinstro with resistivity < 10 Ω/sq) were cut into dimensions of 1.5 cm × 1.0 cm. Subsequent 15-minute ultrasonication with a Helmanex detergent solution and isopropyl alcohol was used to clean the substrates, followed by rinsing with de-ionised (DI) water. They were then blow-dried with nitrogen (N_2) gas and subsequently treated with UV-ozone for 20 minutes to remove any further organic contaminants. A method published by Ngqoloda et al. [19] was used to spin-coat titanium dioxide (TiO_2) onto the FTO to form a glass/FTO/TiO_2 substrate. Lead bromide ($PbBr_2$) thin film was then deposited onto the glass/FTO/TiO_2 substrate via the LPCVD method, similar to that followed by Klue [20].

2.2. Lead halide thin film conversion into a two-dimensional perovskite thin film.

A quartz crucible containing 40 mg of PEAI (CAS-No: 151059-43-7, <= 98% purity, Sigma-Aldrich) salt was placed at the centre of the first zone of a LPCVD tube furnace. The as-prepared $PbBr_2$ thin film was placed horizontally on a silicon wafer in the centre of the second zone. The quartz tube was securely closed on both ends with metal flanges, and the reaction tube was pumped to an initial pressure of 0.01 mbar. The furnace was set to increase the substrate temperature (zone 2), reaching a nominal temperature of 100 °C. Zone 1 was set to heat up to two distinct nominal temperatures of 170 °C and 190 °C.

For each conversion, the temperature was set to dwell at the respective nominal temperatures for 60 minutes. During the conversion process, N_2 gas was set to flow downstream at 100 standard cubic centimetres (SCCM). The conversion pressure was maintained at 1 mbar. Once the 60-minute dwelling time was reached, the substrates were allowed to cool to room temperature under a N_2 flow.

2.3. Characterisation

The film thicknesses were determined using a Dektak 6M stylus thickness profiler; the structural properties of the converted thin film were determined using Empyrean XRD equipment from PANalytical. A copper K-alpha 1 (Cu

$K_{\alpha 1}$) X-ray radiation source with a wavelength of 1.5406 Å was utilised to produce a continuous scan over the range 2θ = 5° - 100° with a step size of 0.02°, a voltage of 45 kV, and a tube current of 40mA, employing a 0.76 mm fixed divergence slit. An Ocean Optics UV spectrophotometer was utilised to measure optical transmission with a spectral resolution of 0.5 nm between 250 and 1000 nm. The room-temperature photoluminescence (PL) spectra of the converted films were measured in a reflection geometry using an excitation light-emitting diode (LED) source set to 365 nm.

3. Results and discussion

3.1. Film thickness

It was found that after converting $PbBr_2$ thin film into a 2D MHP thin film, approximately 10 mg and 30 mg of the initial 40 mg of PEAI had evaporated at conversion temperatures of 170 °C and 190 °C, respectively. The higher PEAI consumption at a 190 °C conversion temperature was due to the increased sublimation rate at higher temperatures, resulting in a higher PEAI vapour concentration during the conversion process. The thickness of the $PbBr_2$ precursor film was determined to be 145 nm. It was observed that exposing the precursor $PbBr_2$ thin film to PEAI vapour increased the film thickness to 478 nm and 853 nm for conversion temperatures of 170 °C and 190 °C, respectively. The thickness increase is due to the diffusion and intercalation of PEAI molecules within the precursor thin films. During the intercalation reaction, the PEA^+ embed themselves between the $[BX_6]^{-4}$ octahedra to form a 2D MHP. Additionally, the thickness increased at 190 °C, which is attributed to the excess supply of PEAI.

3.2. Structural properties

XRD analysis was done on the converted $PbBr_2$ thin films, and the XRD patterns are provided in Figure 1. Diffraction peaks belonging to a 2D perovskite triclinic structure with a p-1 space group were identified. The diffraction peaks start at low angles of 2θ ~ 5.4°, 10.8°, 16.2°, 21.6°, 27.0°, 32.4°and 37.8° are indexed to the (002), (004), (006), (008), (00$\underline{1}$0), (00$\underline{1}$2), and (00$\underline{1}$4) planes, respectively, for both conversion temperatures, which agrees to previous reports [13, 22]. The periodic nature of the (00l) family diffraction peaks at intervals of 2θ ~ 5.4° is evidence that the PEAI diffused into the $PbBr_2$ thin film to intercalate within the $[BX_6]^{-4}$ octahedra, forming a 2D layered perovskite structure (n = 1) [13, 21-23].

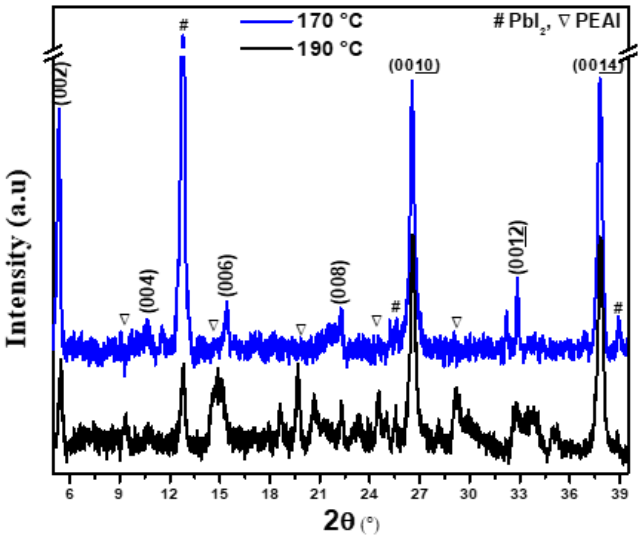

Figure 1. The converted $PbBr_2$ thin-film XRD patterns

The XRD patterns of the converted thin films exhibit additional peaks at 2θ ~ 12.9°, 25.6°, and 38.7°, which were indexed to the (001), (002), and (003) planes, respectively, corresponding to a 2H hexagonal crystal system of lead iodide (PbI_2) with a P-3m1 space group [24]. These PbI_2 diffraction peaks indicate that the iodine (I) ions from the PEAI vapour replace the bromine (Br) ions in the $PbBr_2$ thin film throughout the conversion process.

The ability of 2D MHPs to withstand the intrusion of foreign molecules into the structure is one of their special qualities. This capability may prevent additional diffusion of PEAI molecules into the thin film after the diffusion of PEA^+ ions has reached its capacity, also referred to as the conversion thickness threshold, thereby interrupting the intercalation (conversion) reaction and resulting in the presence of the underlying PbI_2 layer within the converted thin film [13].

At the elevated conversion temperature, a decrease in the 2D MHP and PbI_2 diffraction peak intensity, along with peak broadening, was observed. In addition, higher-intensity diffraction peaks that belong to PEAI were observed in these XRD patterns. This is due to the excess PEAI vapour that condenses on the thin film, as they cannot defuse further due to the conversion thickness threshold.

3.3. Optical properties

Bound electron-hole pairs, known as excitons, can separate into free carriers, which can then be recombined to produce light. About (00l) 2D MHP, there is a modest Stokes shift and narrow emission due to free exciton recombination. Electrons move from the ground state to the excited state when excited by incident radiation, leaving holes in the ground state. The free exciton then recombines, releasing energy in the form of fluorescence [25].

As per the absorption spectra shown in Figure 2(a), the absorption peaks of the converted thin films have been determined to be 2.43 eV and 2.49 eV for the thin films converted at 170 °C and 190 °C, respectively. The fundamental band-edge exciton absorption is responsible for these absorption peaks [26].

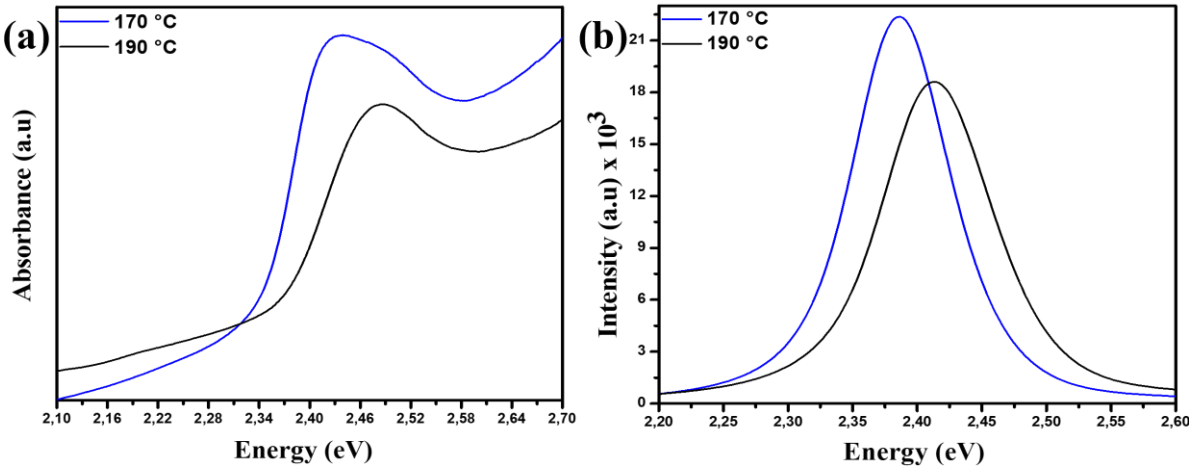

Figure 2. (a) Absorbance spectra of the converted $PbBr_2$ thin films and (b) PL spectra of the converted $PbBr_2$ thin films.

According to the PL spectra shown in Figure 2(b), the PL peaks of the thin films that were converted were calculated to be 2.39 eV and 2.41 eV for the thin films that were converted at 170 °C and 190 °C, respectively. A quenching effect is noticeable at elevated conversion temperature. This may be due to the excess PEAI on the surface, which acts as a quencher by interacting with excited states and dissipating energy non-radiatively, resulting in a decrease in PL intensity.

Yang et al. [23] reported $(PEA)_2PbI_4$ and $(PEA)_2PbBrI_3$ 2D MHP with absorption energies of ~ 2.38 eV and 2.50 eV, respectively. Additionally, they observed PL peaks at ~ 2.37 eV and 2.49 eV, respectively. From this study, it was observed that the absorption and PL peaks are higher than those of the $(PEA)_2PbI_4$ 2D MHP and lower than those of the $(PEA)_2PbBrI_3$ 2D MHP. This suggests that a $(PEA)_2PbBrI_3$ perovskite thin film was not formed; however, the 2D MHP thin films that formed have a stoichiometry of $(PEA)_2PbBr_xI_{4-x}$ ($0 \leq x < 1$).

The Stokes shift is the difference between the positions of the band maxima of the absorption and that of PL emission at the same electronic transition. The slight Stokes shifts of 53.07 meV and 75.48 meV were determined for the thin films converted at 170 °C and 190 °C, respectively, suggesting that the emission originates almost entirely from the recombination of intrinsic excitons, which indicates a low defect density. However, a slight increase of 22.41 meV in the thin film converted at the elevated temperature indicates that the excess PEAI increases the defect density.

According to the Tauc plot shown in Figure 3(a), the band gap (E_g) of the converted thin film was determined to be 2.38 eV for thin films converted at 170 °C and 2.36 eV for thin films converted at 190 °C. The higher E_u, which denotes within the band edge, is the cause of the thin film's lower E_g when converted at a higher conversion temperature.

The Urbach energy (E_u) was calculated from the linear region shown in bold in Figure 3(b). E_u was estimated to be 84.89 meV and 135.96 meV for the thin film converted at 170 °C and 190 °C, respectively. The optical band edge is defined by the E_u, which may be the broadening of the PL peak, suggesting that the elevated conversion temperature increases the defect density as a result of the excess PEAI, introducing alternating vibronic structures [28], and is complemented by the Stokes shift.

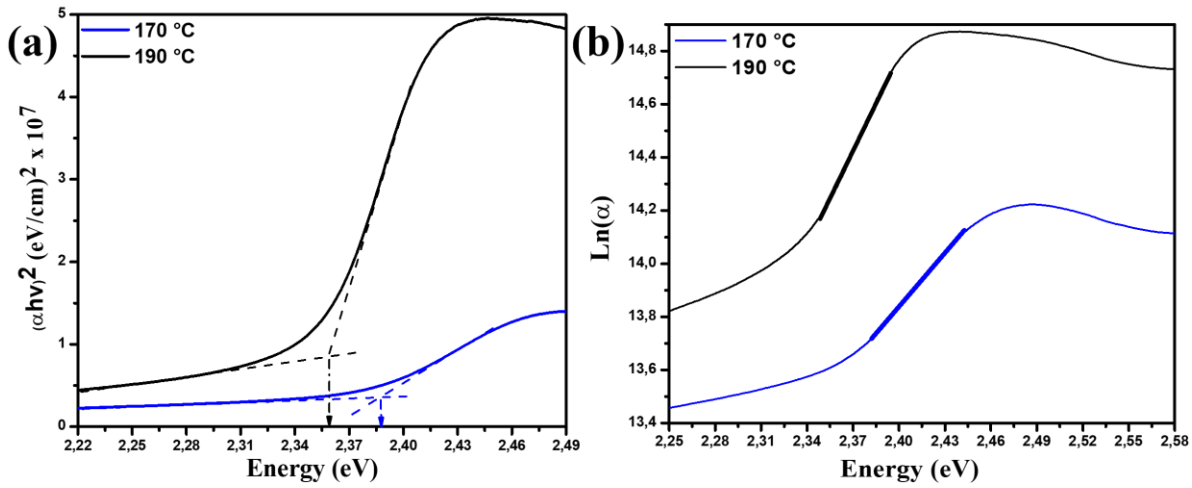

Figure 3. (a) Urbach energy plot of the converted thin films and (b) Tauc plot of the converted thin films.

4. Conclusion

The PBr_2 thin films were then exposed to PEAI vapour, which converted them into 2D MHP. To investigate the impact of conversion temperature, the substrate temperature was set to 100 °C, the source temperature was set to two distinct temperatures of 190 °C and 170 °C, and the conversion was allowed to dwell for 60 minutes. The XRD analysis revealed 2D MHP peaks, which were more intense for the thin films converted at 170 °C. These peaks indicated that the thin films had undergone partial conversion, as evidenced by the presence of PbI_2 peaks. It was observed that the thin films converted at 170 °C had a smaller E_u than the thin films converted at 190 °C. The ideal conversion temperature was determined to be 170 °C. The 2D MHPs can be incorporated into heterostructures to enhance the performance of photovoltaic devices.

References

[1] A. Kojima, K. Teshima, Y. Shirai, and T. Miyasaka, "Organometal halide perovskites as visible-light sensitisers for photovoltaic cells," *Journal of the american chemical society.*, 6;131(17):6050-1, May. 2009.

[2] (NREL), N.R.E.L. "Solar Cell Efficiency Chart," Sep. 2023. [online]. Available: https://www.nrel.gov/pv/cell-efficiency.html.

[3] N. G. Park, "Organometal perovskite light absorbers toward a 20% efficiency low-cost solid-state mesoscopic solar cell," *The Journal of Physical Chemistry Letters*., 1;4(15):2423-9, Aug. 2013.

[4] L. Cheng, T. Jiang, Y. Cao, C. Yi, N. Wang, W. Huang, and J. Wang, "Multiple-quantum-well perovskites for high-performance light-emitting diodes," *Advanced Materials.*, 32(15):1904163, Apr. 2020.

[5] Q. Zhang., et al, "Advances in small perovskite-based lasers," *Small Methods.,* 1(9):1700163, Sep. 2017.

[6] P. Roy, N. K. Sinha, S. Tiwari, and A. Khare, "A review on perovskite solar cells: Evolution of architecture, fabrication techniques, commercialisation issues and status," *Solar Energy.*, 198:665-88, Mar. 2020, doi: 10.1016/j.solener.2020.01.080.

[7] N. S. Kumar, and K. C. Naidu, "A review on perovskite solar cells (PSCs), materials and applications," *Journal of Materiomics.*, 1;7(5):940-56, Sep. 2021, doi: 10.1016/j.jmat.2021.04.002.
[8] R. Wang., et al, "A review of perovskites solar cell stability," *Advanced Functional Materials.*, 29(47):1808843, Nov. 2019, doi: 10.1002/adfm.201808843.
[9] W. Fu., et al, "Stability of perovskite materials and devices," *Materials Today.,* 1;58:275-96, Sep. 2022, doi: 10.1016/j.mattod.2022.06.020.
[10] S. Chen, X. Dai, S. Xu, H. Jiao, L. Zhao, and J. Huang, "Stabilising perovskite-substrate interfaces for high-performance perovskite modules," *Science.*, 20;373(6557):902-7, Aug. 2021, doi: 10.1126/science.abi6323.
[11] J. W. Lee., et al, "2D perovskite stabilised phase-pure formamidinium perovskite solar cells," *Nature communications.*, 1;9(1):3021, Aug. 2018, doi; 10.1038/s41467-018-05454-4.
[12] Z. Yang., et al, "Stabilised wide bandgap perovskite solar cells by tin substitution," *Nano letters.*, 14;16(12):7739-47, Dec. 2016, doi: 10.1021/acs.nanolett.6b03857.
[13] S. S. Magubane, R. Burns, S. Ngqoloda, C. J. Oliphant, P. F. Miceli, and C. J. Arendse, "Sequential chemical vapor deposition of two-dimensional Sn–Pb compound perovskite thin films and its exciton transport," *ACS Applied Electronic Materials.*, 5;5(10):5352-61, Jul. 2023, doi: 10.1021/acsaelm.3c00266.
[14] X. Zhang., et al, "Orientation regulation of phenylethylammonium cation based 2D perovskite solar cell with efficiency higher than 11%," *Advanced Energy Materials.*, 8(14):1702498, May. 2018, doi: 10.1002/aenm.201702498.
[15] L. Zhang., et al, "High-performance quasi-2D perovskite light-emitting diodes: from materials to devices," *Light: Science & Applications.*, 19;10(1):61, Mar 2021, doi: 10.1038/s41377-021-00501-0.
[16] X. Chen, H. Zhou, and H. Wang, "2D/3D halide perovskites for optoelectronic devices," *Frontiers in Chemistry.*, 19;9:715157, Aug. 2021, doi; 10.3389/fchem.2021.715157.
[17] M. Ren, S. Cao, J. Zhao, B. Zou, and R. Zeng, "Advances and challenges in two-dimensional organic–inorganic hybrid perovskites toward high-performance light-emitting diodes," *Nano-Micro Letters.*, 13(1):163, Dec. 2021, doi: 10.1007/s40820-021-00685-5.
[18] K. Wang, J. Y. Park, Akriti, and L. Dou, "Two-dimensional halide perovskite quantum-well emitters: A critical review," *EcoMat.*, 3(3):e12104, Jun. 2021, doi: 10.1002/eom2.12104.
[19] S. Ngqoloda, C. J. Arendse, T. F. Muller, F. R. Cummings, and C. Oliphant, "Effect of HTL thickness on air processed CVD perovskite solar cells," *Materials Today: Proceedings.*, 1;36:303-8, Jan. 2021, doi: 10.1016/j.matpr.2020.04.074.
[20] S. C. Klue, "Optimisation of lead halide perovskite thin films by chemical vapour deposition," M.S. thesis, Dept. Phy., UWC., CPT, 2021.
[21] Y.A. Chen. et al, "Effect of the Large-Size A-Site Cation on the Crystal Growth and Phase Distribution of 2D/3D Mixed Perovskite Films via a Low-Pressure Vapor-Assisted Solution Process," *The Journal of Physical Chemistry C.*, 28;125(48):26601-12, Nov. 2021, doi: 10.1021/acs.jpcc.1c07795.
[22] S. Yang., et al, "Ultrathin two-dimensional organic–inorganic hybrid perovskite nanosheets with bright, tunable photoluminescence and high stability," *Angewandte Chemie.*, 3;129(15):4316-9, Apr. 2017, doi: 10.1002/ange.201701134.
[23] A. Zanetta., et al, "Manipulating color emission in 2D hybrid perovskites by fine tuning halide segregation: a transparent green emitter," *Advanced Materials.*, 34(1):2105942, Jan. 2022, doi: 10.1002/adma.202105942.
[24] H. Sun., et al, "Morphological and structural evolution during thermally physical vapor phase growth of PbI2 polycrystalline thin films," *Journal of crystal growth.*, 1;405:29-34, Nov. 2014, doi: 10.1016/j.jcrysgro.2014.07.043.
[25] X. Gao., et al, "Ruddlesden–popper perovskites: synthesis and optical properties for optoelectronic applications," *Advanced Science.*, 6(22):1900941, doi; 10.1002/advs.201900941.
[26] T. Zhang., et al, "Regulation of the luminescence mechanism of two-dimensional tin halide perovskites," *Nature communications.,* 2022 10;13(1):60, Jan. 2022, doi: 10.1038/s41467-021-27663-0.
[27] M. G. La-Placa., et al, "Dual-source vacuum deposition of pure and mixed halide 2D perovskites: thin film characterisation and processing guidelines," *Journal of Materials Chemistry C.*, 8(6):1902-8, 2022
[28] T. B. Ren., et al, "A general method to increase stokes shift by introducing alternating vibronic structures," *Journal of the American Chemical Society.,* 24;140(24):7716-22, May. 2018.